

A model order reduction based adaptive parareal method for time-dependent partial differential equations [★]

Xiaoying Dai^{a,*}, Miao Hu^b, Shuwei Shen^a

^a*State Key Laboratory of Mathematical sciences, Academy of Mathematics and Systems Science, Chinese Academy of sciences, Beijing 100190, China; and School of Mathematical Sciences, University of Chinese Academy of Sciences, Beijing 100049, China*

^b*China Pharmaceutical University, Nanjing 211198, China*

Abstract

In this paper, we propose a model order reduction based adaptive parareal method for time-dependent partial differential equations. By using the data obtained by the fine propagator in each iteration of the plain parareal method together with some model order reduction technique, we construct the coarse propagator adaptively in each parareal iteration, and then obtain our adaptive parareal method. We apply this new method to solve some 3D time-dependent advection–diffusion equations with the Kolmogorov flow and the ABC flow. Numerical results show the good performance of our method in simulating long-term evolution problems.

Keywords: parareal method, adaptive, model order reduction, propagator, advection-diffusion equation, long-term evolution

1. Introduction

With an increasing number and efficiency of cores in supercomputer platforms, there is a growing demand for scalability and parallelism of algorithms. However, when dealing with time-dependent problems, the inherent sequential nature of the time direction becomes a bottleneck for scalability. To overcome this obstacle, people attempt to extend parallelism into the time direction. We refer to [20, 24] and references therein for an overview of the development of parallel in time methods. One of the most widely used methods is the parareal method.

The parareal method was first proposed in [30]. The main idea is to break the problem defined over the entire time interval into separate subproblems on time subintervals. After that, some analysis on the convergence and the stability for the parareal method is given in [4, 21, 23, 39]. Over the past few years, the parareal method has

[★]This work was supported by the National Natural Science Foundation of China under grant 92270206 and the Strategic Priority Research Program of the Chinese Academy of Sciences under grant XDB0640000.

*Corresponding author: email: daixy@lsec.cc.ac.cn;

Email addresses: humiao@cpu.edu.cn (Miao Hu), shenshuwei@lsec.cc.ac.cn (Shuwei Shen)

been used widely in many fields (see [32] for a review), e.g., fluid and structure problems [18], the Navier-Stokes equations [19], reservoir simulation [25], the simulation of molecular dynamics [29], time-periodic problems [22] and so on. In further, some modified parareal methods have been proposed to deal with the long time simulation of hyperbolic problems and Hamiltonian systems[5, 16, 17, 18], which are shown to have better convergence and stability.

The parareal method involves two propagators: a fine propagator with high accuracy but expensive computational cost that computes in parallel on time subintervals, and a coarse propagator that is inexpensive to compute over the entire time interval. The choice of the fine propagator depends on the specific problem and the expected accuracy for the approximate solution. The fine propagator usually applies a classical time integrator (e.g., Euler or Runge-Kutta methods) with a fine step size, combined with a classical spatial discretization method that has fine spatial resolution. The classical spatial discretization methods include the finite element method (FEM) [9], the finite difference method (FDM) [40] and so on. These methods often result in semi-discretized systems with very large dimensionality, particularly for problems with high spatial dimension, leading to computationally intensive tasks involving millions or billions of degrees of freedom.

Meanwhile, the choice of the coarse propagator is more flexible, which also has an important impact on the performance of the parareal method. Numerical analysis [4, 21, 23] demonstrates the effect of the accuracy of the coarse propagator on the convergence speed of the parareal method: the higher accuracy of the coarse propagator, the faster the parareal method converges. However, a coarse propagator with high accuracy often results in expensive computational cost. Therefore, developing a coarse propagator with adequate accuracy and low cost is significant for improving the performance of the parareal method. In other words, a good coarse propagator usually needs to satisfy the following two principles: sufficient accuracy and low computational cost. The most commonly used coarse propagator is the same scheme as that used in the fine propagator but with a coarser step size [30]. Additionally, the coarse propagator can employ an explicit time discretization scheme [35] or a scheme with lower order accuracy [7]. Meanwhile, there are some works on using neural networks, simplified physics modules or model order reduction to construct the coarse propagators [3, 11, 12, 27, 28, 29, 34, 37].

For the plain parareal method, the accuracy of both the coarse and fine propagator are usually fixed throughout all iterations. To further accelerate the convergence and improve the efficiency, several adaptive parareal methods have been proposed in recent years. In [33], Maday et al. introduced an adaptive parareal method by improving the accuracy of the fine propagator during iterations incrementally, and also analyzed the convergence and parallel efficiency. In [29], Legoll et al. proposed an adaptive variant by dividing the entire time interval into smaller time-slabs adaptively, and applied it to the simulation of molecular dynamic trajectories.

In this article, we aim to design an adaptive parareal method for time-dependent partial differential equations by updating the coarse propagator adaptively during the iterations. As mentioned earlier, the computational cost of the coarse propagator is determined by both temporal and spatial discretization. For temporal discretization, we employ the same time integrator used in the fine propagator but with a coarse step

size. For spatial discretization, we note that in each iteration of the parareal method, we need to propagate the fine propagator on each time subinterval, which will provide a large amount of data. Our basic idea is trying to make use of the data to construct a subspace, which will serve as the discrete space for the coarse propagator. As the parareal iteration proceeds, the iterative solution becomes increasingly close to the solution obtained by applying the fine propagator starting from the exact initial value. The subspace constructed from the data may thus capture the behavior of the fine-scale solution better and better. Therefore, we have reason to believe that as the iteration proceeds, the spatial discretization accuracy of the coarse propagator will approach to that of the fine propagator's spatial discretization. Furthermore, to reduce the cost of the coarse propagator, we hope the dimension of the subspace constructed from the data can be as small as possible. To achieve this, we employ some model order reduction technique [6, 13, 31] to construct a subspace from the data. Specifically, we employ the proper orthogonal decomposition (POD) [38] to perform the model order reduction in this article.

The main steps for our adaptive parareal method for time-dependent PDEs are as follows: at first, using the data obtained from the fine propagator on the early time interval and the POD method, we initialize the coarse propagator by constructing its POD subspace for discretization. The initial values on each time subinterval are then obtained by sequentially propagating the coarse propagator over the entire time interval. During the k -th iteration with $k \geq 1$, we first solve the subproblem by the fine propagator on each time subinterval and collect snapshots in parallel, and then update the POD subspace on each time subinterval in parallel using these snapshots, from which we can refine the coarse propagator iteratively. In further, we augment these subspaces by adding the initial values of the subproblems on time subintervals. This step can improve the accuracy of the coarse propagator by removing the error introduced by Galerkin projection. Finally, we obtain more accurate numerical solutions by using this coarse propagator with higher accuracy. This process establishes a positive feedback loop, wherein the coarse propagator improves progressively, leading to increasingly accurate approximate solutions obtained by the parareal method.

The remainder of this paper is organized as follows. We review some fundamental concepts of the parareal method in section 2. In section 3, we introduce the details on how to construct our adaptive parareal method, especially those on how to use data obtained from propagating the fine propagator in each time subinterval together with the POD method to construct the POD subspace which will be used as the spatial discretization of the coarse propagator, and the analysis of the speed-up and computational complexity for our adaptive parareal method. In section 4, we apply our method to some typical time-dependent partial differential equations, i.e., the advection-diffusion equations with three dimensional velocity fields, including both the Kolmogorov flow and the ABC flow. The numerical results indicate that our method performs well in simulating the long-term evolution of this kind of problem, especially for the advection-dominated cases. Finally, we present our concluding remarks in section 5.

2. Preliminaries

In this paper, we use bold letters to denote matrices and vectors, and regular letters for functions and scalars. Some standard notation for Sobolev spaces is also used, see e.g., [41]. Let V be a Banach space with norm $\| \cdot \|_V$ and V^* be the dual space of V . We first introduce the Banach space

$$W^2(0, T; V, V^*) = \left\{ u \in L^2(0, T; V) \mid \frac{\partial u}{\partial t} \in L^2(0, T; V^*) \right\},$$

where $L^p(0, T; V) = \left\{ u : (0, T) \rightarrow V \mid u \text{ is measurable and } \int_0^T \|u(t)\|_V^p dt < \infty \right\}$. $\frac{\partial u}{\partial t}$ is the partial derivative with respect to time in the distributional sense. We call $u \in C(0, T; V)$ if

$$\lim_{t \rightarrow t_0} \|u(t) - u(t_0)\|_V = 0, \quad \forall t_0 \in [0, T]$$

with $\|u\|_{C(0, T; V)} = \max_{t \in [0, T]} \|u(t)\|_V$.

We consider the following time-dependent partial differential equations with periodic boundary conditions

$$\begin{aligned} \frac{\partial u(x_1, \dots, x_d, t)}{\partial t} + \mathcal{A}(t, u(x_1, \dots, x_d, t)) &= f(x_1, \dots, x_d), \quad \text{in } \Omega \times (0, T] \\ u(x_1, \dots, x_d, 0) &= u_0(x_1, \dots, x_d), \quad \text{in } \Omega \\ u(x_1 + L_1, x_2, \dots, x_d, t) &= u(x_1, x_2, \dots, x_d, t), \quad \text{on } \partial\Omega \times (0, T] \quad (1) \\ &\dots \\ u(x_1, x_2, \dots, x_d + L_d, t) &= u(x_1, x_2, \dots, x_d, t), \quad \text{on } \partial\Omega \times (0, T] \end{aligned}$$

in a bounded space-time cylinder $\Omega \times [0, T] \subset \mathbb{R}^d \times [0, T]$, $d \geq 2$, where $\Omega := [0, L_1] \times \dots \times [0, L_d]$. Let

$$V = \left\{ v \in H^1(\Omega) \mid v \text{ satisfies the boundary conditions in (1)} \right\},$$

$u_0 \in V$ and $f \in L^2(0, T; V)$. The final time T is arbitrary but fixed in what follows. \mathcal{A} is a partial differential operator, possibly nonlinear, from $[0, T] \times H^1(\Omega)$ into its dual space $H^{-1}(\Omega)$.

Then we assume the problem is well-posed with sufficient regularity, and denote the solution of (1) as $u \in W^2(0, T; V, V^*)$. All methods introduced later are not limited to any special boundary conditions, with only minor adjustments required in the definition of the bilinear form for different boundaries.

We begin with a brief review of the parareal method, which was first proposed in [30]. The exact propagator $\mathcal{E} : [0, T] \times [0, T] \times V \rightarrow V$ is defined as follows:

$$u(t) = \mathcal{E}(s, t, u(s)), \quad s \leq t,$$

where $u(s)$ represents the solution at time s . Let

$$0 = t_0 < t_1 < t_2 < \dots < t_n < t_{n+1} < \dots < t_N = T$$

be a uniform partition of the time domain $[0, T]$, where $t_n = n \cdot \Delta T$, $\Delta T = \frac{T}{N}$. Then we have

$$u(t_{n+1}) = \mathcal{E}(t_n, t_{n+1}, u(t_n)), \quad n = 0, \dots, N-1.$$

Let the fine propagator \mathcal{F} be an approximation of \mathcal{E} with high resolution. Both the exact and fine propagators are essentially sequential. Let \mathcal{G} be a coarse propagator, which has lower computational cost and lower accuracy compared with the fine propagator \mathcal{F} .

Denote k the index of iteration, the parareal method [30] builds a sequence of N -tuples $\{U_n^k\}$ iteratively by the following formula:

$$\begin{cases} U_{n+1}^0 = \mathcal{G}(t_n, t_{n+1}, U_n^0), & U_0^0 = u_0, \quad n = 0, 1, \dots, N-1, \\ U_{n+1}^k = \mathcal{G}(t_n, t_{n+1}, U_n^k) + \mathcal{F}(t_n, t_{n+1}, U_n^{k-1}) - \mathcal{G}(t_n, t_{n+1}, U_n^{k-1}), & U_0^k = u_0, \quad n = 0, 1, \dots, N-1, \\ k = 1, 2, \dots. \end{cases} \quad (2)$$

This method breaks the original problem defined over the entire time interval $[0, T]$ into N separate subproblems on time subintervals $[t_n, t_{n+1}]$. During the k -th iteration, we first obtain $\mathcal{F}(t_n, t_{n+1}, U_n^{k-1})$ by propagating the fine propagator starting from t_n with initial value U_n^{k-1} to t_{n+1} in each time subinterval $[t_n, t_{n+1}]$. Since U_n^{k-1} are obtained from the last iteration, the calculation of $\mathcal{F}(t_n, t_{n+1}, U_n^{k-1})$ can be carried out in parallel. After this step, since $\mathcal{G}(t_n, t_{n+1}, U_n^{k-1})$ can be obtained from the previous iteration, we only need to calculate $\mathcal{G}(t_n, t_{n+1}, U_n^k)$ and update U_{n+1}^k sequentially.

It is obvious that within at most N iterations, the parareal method will converge to the solution obtained sequentially by the fine propagator in the whole time domain. However, it is desirable for the method to be able to achieve the convergence in significantly fewer than N iterations. Otherwise, no speed-up will be obtained.

3. Adaptive parareal method based on model order reduction

In this section, we propose our adaptive parareal method, which is essentially different from the existing works. Previous studies [4, 21, 23] show that the convergence rate of the parareal method depends critically on the accuracy of the coarse propagator. The higher accuracy of the coarse propagator yields faster convergence of the parareal method. However, high accuracy also means high computational cost. This trade-off highlights the importance of developing computationally efficient coarse propagators that maintain sufficient accuracy for improving the performance of the parareal method.

Usually, the resolution of the coarse propagator remains fixed throughout all iterations in the existing works. To accelerate the convergence, we propose a method that can improve the accuracy of the coarse propagator adaptively while maintaining low computational cost. This adaptive parareal method can be expressed as the following general formula:

$$\begin{cases} U_{n+1}^0 = \mathcal{G}_0(t_n, t_{n+1}, U_n^0), & U_0^0 = u_0, \\ U_{n+1}^k = \mathcal{G}_k(t_n, t_{n+1}, U_n^k) + \mathcal{F}(t_n, t_{n+1}, U_n^{k-1}) - \mathcal{G}_k(t_n, t_{n+1}, U_n^{k-1}), & U_0^k = u_0, \\ k = 1, 2, \dots. \end{cases} \quad (3)$$

Unlike the plain parareal method (2), where the coarse propagator \mathcal{G} is not changed during all iterations. Here, at different iterations, the coarse propagator may be different. Most importantly, the accuracy of the coarse propagator is expected to increase adaptively as the iteration proceeds. We notice that during each parareal iteration, the propagating of the fine propagator on each time subinterval produces a large amount of data, which is in fact an approximation to the solution obtained by applying the fine propagator starting from the exact initial value, with increasing accuracy over iterations. Therefore, we consider to use the data to construct the spatial discretization of the coarse propagator. We believe that as the iteration proceeds, the spatial discretization accuracy of the coarse propagator can approach to that of the fine propagator's spatial discretization progressively. Moreover, to minimize the computational cost of the coarse propagator, we aim to construct the lowest-dimensional subspace from the data. Thanks to the model order reduction methods [6, 13, 31], we can achieve this successfully. Specifically, we employ the proper orthogonal decomposition (POD) [38] to perform the model order reduction in this article.

Roughly speaking, the main process for constructing the coarse propagator is as follows. In the 0-th iteration, we first apply the fine propagator to the initial part of the time domain to generate the data, which is then used to construct the POD subspace for the coarse propagator. We then propagate the coarse propagator over the entire time interval to provide the initial values for the subproblems on time subintervals. In subsequent iterations, we parallelize the fine propagator across all time subintervals and collect snapshots. These snapshots are then used to update the POD subspace in parallel, leading to a refined coarse propagator. Furthermore, to improve accuracy, we augment the updated subspaces with the initial values from each time subinterval, thereby eliminating the Galerkin projection errors.

In the remainder of this section, we will introduce the details on how to apply the adaptive parareal method (3) to deal with problem (1).

We take an inner product with $v \in V$ in (1) and define (\cdot, \cdot) as the the inner product in $L^2(\Omega)$. We then obtain the variational form of (1) as follows: find $u \in W^2(0, T; V, V^*)$ such that $u(0) = u_0 \in V^*$ and for almost every $t \in (0, T)$,

$$\left(\frac{\partial u}{\partial t}, v \right) + (\mathcal{A}(t, u), v) = (f, v), \quad \forall v \in V. \quad (4)$$

We first introduce the temporal discretization of (4). In this article, we choose the implicit Euler scheme [2] as the temporal discretization for both the fine and coarse propagators, but with time step sizes δt and dT respectively. We take the fine propagator as an example to introduce the details of the temporal discretization. Let $u_n \in V$ be the approximation of $u(n\delta t)$. Applying the implicit Euler scheme to (4), then we can get the following semi-discretization scheme:

$$\left(\frac{u_n - u_{n-1}}{\delta t}, v \right) + (\mathcal{A}(n\delta t, u_n), v) = (f_n, v), \quad \forall v \in V. \quad (5)$$

The temporal discretization of (4) by coarse propagator is the same as (5) but with time step δt being replaced by dT .

In the following part of this section, we will introduce the spatial discretization of the fine propagator and coarse propagator respectively.

3.1. Spatial discretization of the fine propagator

For simplicity, the iteration index k will be omitted in this subsection. For the spatial discretization of the fine propagator, we choose the standard finite element discretization [9]. Let \mathcal{T}_h be a family of nested, shape-regular conforming meshes over Ω with mesh size h , i.e., there exists a constant γ^* such that

$$\frac{h_\tau}{\rho_\tau} \leq \gamma^*, \quad \forall \tau \in \mathcal{T}_h,$$

where h_τ is the diameter of τ for each $\tau \in \mathcal{T}_h$, ρ_τ is the diameter of the biggest ball contained in τ , and $h = \max \{h_\tau : \tau \in \mathcal{T}_h\}$. Denote the finite element space on Ω corresponding to mesh \mathcal{T}_h as V_h ,

$$V_h = \left\{ v_h : v_h|_\tau \in \mathbb{P}_\tau, \forall \tau \in \mathcal{T}_h \text{ and } v_h \in C^0(\bar{\Omega}) \right\},$$

where \mathbb{P}_τ is a set of polynomials on element τ . Let $\{\phi_{h,1}, \phi_{h,2}, \dots, \phi_{h,N_g}\}$ be a basis of V_h , where N_g is the dimension of V_h . Let

$$\Phi_h := (\phi_{h,1}, \phi_{h,2}, \dots, \phi_{h,N_g}), \quad (6)$$

and $u_{h,n} \in V_h$ be the approximation of $u(n\delta t)$. We then obtain the following full-discretized problem: find $\{u_{h,n}\}_{n=1,2,\dots,N}$ with each $u_{h,n} \in V_h$, such that

$$\left(\frac{u_{h,n} - u_{h,n-1}}{\delta t}, v_h \right) + (\mathcal{A}(n\delta t, u_{h,n}), v_h) = (f_n, v_h), \quad v_h \in V_h. \quad (7)$$

Note that each $u_{h,n}$ can be expressed as

$$u_{h,n} = \sum_{i=1}^{N_g} a_{n,i} \phi_{h,i}, \quad (8)$$

where $a_{n,i} \in \mathbb{R}$. Inserting (8) into (7), and choosing $v_h = \phi_{h,j}$, $j = 1, 2, \dots, N_g$, we obtain

$$\left(\sum_{i=1}^{N_g} a_{n,i} \phi_{h,i} - \sum_{i=1}^{N_g} a_{n-1,i} \phi_{h,i}, \phi_{h,j} \right) + \delta t \cdot \left(\mathcal{A}(n\delta t, \sum_{i=1}^{N_g} a_{n,i} \phi_{h,i}), \phi_{h,j} \right) = \delta t \cdot (f_n, \phi_{h,j}). \quad (9)$$

Denoting

$$\mathbf{u}_{h,n} = (a_{n,1}, a_{n,2}, \dots, a_{n,N_g})^\top, \quad \mathbf{A}_{h,n,i,j} = (\phi_{h,j}, \phi_{h,i}) + \delta t \cdot (\mathcal{A}(n\delta t, \phi_{h,j}), \phi_{h,i}),$$

$$\mathbf{b}_{h,n,i} = \delta t \cdot (f_n, \phi_{h,i}),$$

we then obtain the following algebraic form

$$\mathbf{A}_{h,n} \mathbf{u}_{h,n} = \mathbf{b}_{h,n} + \mathbf{M} \mathbf{u}_{h,n-1}, \quad (10)$$

where $\mathbf{A}_{h,n} = (\mathbf{A}_{h,n,ij})_{N_g \times N_g}$, $\mathbf{b}_{h,n} = (\mathbf{b}_{h,n,i})_{N_g}$, and $\mathbf{M} = (\phi_{h,j}, \phi_{h,i})_{N_g \times N_g}$ is the mass matrix.

3.2. Adaptive spatial discretization of the coarse propagator

It is well-known that to make the parareal method efficient, the coarse propagator should be cheap enough. Therefore, we do not employ the spatial discretization used in the fine propagator, i.e., the finite element method, for the coarse propagator. Instead, following [14, 15], we employ the POD method for the spatial discretization of the coarse propagator. That is, during the propagation using the coarse propagator, we will discretize the problem in a subspace spanned by some POD modes, whose dimension is usually much smaller than that of the finite element space. As stated in the introduction, to improve the performance of the parareal method, we hope the accuracy of coarse propagator can be as high as possible. In the following of this subsection, we will introduce the details on how we update the POD subspace to improve the accuracy of the spatial discretization of the coarse propagator adaptively. As mentioned at the beginning of this section, the basic idea for constructing the spatial discretization for the coarse propagator is to make use of the data obtained by the fine propagator in each parareal iteration, together with some model order reduction technique, to update the subspace for the spatial discretization. Our introductions are separated into two cases: spatial discretization of the coarse propagator at the beginning of the parareal iteration($k = 0$) and the adaptive update of the subspace for spatial discretization of the coarse propagator for each k -th parareal iteration with $k \geq 1$.

Case I: Spatial discretization of the coarse propagator for k -th parareal iteration with $k = 0$

For the 0-th iteration, we use the POD method to do the spatial discretization of the coarse propagator. That is, we first propagate (1) on time interval $[0, T_0]$ using the fine propagator, then use the snapshots obtained to construct some POD subspace, and use this POD subspace as the spatial discretization of the coarse propagator \mathcal{G}_0 . After that, on time interval $[T_0, T]$, we propagate (1) by the coarse propagator \mathcal{G}_0 . More details on how to use POD method to solve the time-dependent partial differential equations can be found in [14, 15].

Now we introduce the details for each step. At first, we discretize (5) on $[0, T_0]$ by the fine propagator, and collect the numerical solutions at different times $t = 0, \delta M \delta t, \dots, (n_s - 1) \delta M \delta t$ as a snapshot matrix $\mathbf{W}_h \in \mathbb{R}^{N_g \times n_s}$. Here, δM is an integer parameter and $n_s = \lfloor \frac{T_0}{\delta t \cdot \delta M} \rfloor + 1$, where $\lfloor \cdot \rfloor$ means the round down. The approximation of the solution at T_0 is denoted as \hat{u}_0 . Then we use \mathbf{W}_h to construct the POD modes. For details on how to construct the POD modes from existing data, please refer to [42]. We first solve the eigenvalue problem of the symmetric positive definite matrix $(\mathbf{W}_h)^\top \mathbf{M} \mathbf{W}_h$ and obtain the eigenvalues $\lambda_1 \geq \lambda_2 \geq \dots \geq \lambda_r > \lambda_{r+1} = \dots = \lambda_{n_s} = 0$, together with the eigenvectors corresponding to the nonzero eigenvalues, denoted by $\mathbf{Y} = [\mathbf{y}_1, \mathbf{y}_2, \dots, \mathbf{y}_r] \in \mathbb{R}^{n_s \times r}$. Then we obtain the POD modes $\mathbf{R} = [\mathbf{r}_1, \mathbf{r}_2, \dots, \mathbf{r}_r] \in \mathbb{R}^{N_g \times r}$ by $\mathbf{r}_i = \frac{1}{\sqrt{\lambda_i}} \mathbf{W}_h \mathbf{y}_i$. Setting $\gamma_1 \in (0, 1]$ as a given parameter, the dimension of the POD subspace is

$$m = \min \left\{ k \mid \sum_{i=1}^k \sqrt{\lambda_i} \geq \gamma_1 \cdot \sum_{i=1}^r \sqrt{\lambda_i} \right\}.$$

Denote $\tilde{\mathbf{R}} = \mathbf{R}[:, 1:m]$ as the first m columns of \mathbf{R} . Then we obtain the POD modes

$$\Psi_h := (\psi_{h,1}, \psi_{h,2}, \dots, \psi_{h,m}) = \Phi_h \tilde{\mathbf{R}},$$

and its corresponding POD subspace V_{POD}^0 , here Φ_h is defined in (6). Then, we finish the construction of the POD subspace V_{POD}^0 for the spatial discretization of the coarse propagator \mathcal{G}_0 . We summarize the process for constructing POD modes as a routine $\text{POD_Mode}(\mathbf{W}_h, \gamma, \mathbf{M}, \Phi_h, m, \Psi_h, \tilde{\mathbf{R}})$ in Algorithm 1, see also in [14, 15].

Algorithm 1 $\text{POD_Mode}(\mathbf{W}_h, \gamma, \mathbf{M}, \Phi_h, m, \Psi_h, \tilde{\mathbf{R}})$

Input: $\mathbf{W}_h, \gamma, \mathbf{M}, \Phi_h = (\phi_{h,1}, \phi_{h,2}, \dots, \phi_{h,N_g})$.

Output: m , POD modes $\Psi_h = (\psi_{h,1}, \psi_{h,2}, \dots, \psi_{h,m})$, $\tilde{\mathbf{R}}$.

- 1: Solve the eigenvalue problem of $(\mathbf{W}_h)^T \mathbf{M} \mathbf{W}_h$ and obtain \mathbf{R} .
- 2: Let $m = \min \left\{ k \mid \sum_{i=1}^k \sqrt{\lambda_i} \geq \gamma_1 \cdot \sum_{i=1}^r \sqrt{\lambda_i} \right\}$.
- 3: $\tilde{\mathbf{R}} = \mathbf{R}[:, 1:m]$.
- 4: $\Psi_h = (\psi_{h,1}, \psi_{h,2}, \dots, \psi_{h,m}) = \Phi_h \tilde{\mathbf{R}}$.

Next, we show how to discretize (5) in V_{POD}^0 for $t \geq T_0$. We first set $u_{l,\text{POD}} = \sum_{j=1}^m \alpha_{l,j} \psi_{h,j}$, as the approximation of $u(T_0 + ldT)$, and $\mathbf{u}_{l,\text{POD}} = (\alpha_{l,1}, \dots, \alpha_{l,m})^T$, $\alpha_{l,j} \in \mathbb{R}$. Define

$$\mathbf{A}_{l,\text{POD},ij} = (\psi_{h,j}, \psi_{h,i}) + dT \cdot (\mathcal{A}(T_0 + ldT, \psi_{h,j}), \psi_{h,i}), \quad \mathbf{b}_{l,\text{POD},i} = dT \cdot (f_n, \psi_{h,i}),$$

we arrive at the reduced algebraic form (11)

$$\mathbf{A}_{l,\text{POD}} \mathbf{u}_{l,\text{POD}} = \mathbf{b}_{l,\text{POD}} + \mathbf{M}_{\text{POD}} \mathbf{u}_{l-1,\text{POD}}, \quad (11)$$

where $\mathbf{A}_{l,\text{POD}} = (\mathbf{A}_{l,\text{POD},ij})_{m \times m}$, $\mathbf{b}_{l,\text{POD}} = (\mathbf{b}_{l,\text{POD},i})_m$ and $\mathbf{M}_{\text{POD}} = (\psi_{h,j}, \psi_{h,i})_{m \times m}$. Considering that the POD modes can be expressed in $\Psi_h = \Phi_h \tilde{\mathbf{R}}$, we can also write the equation (11) as

$$\tilde{\mathbf{R}}^T \mathbf{A}_{h,l} \tilde{\mathbf{R}} \mathbf{u}_{l,\text{POD}} = \tilde{\mathbf{R}}^T \mathbf{b}_{h,l} + \tilde{\mathbf{R}}^T \mathbf{M} \tilde{\mathbf{R}} \mathbf{u}_{l-1,\text{POD}}. \quad (12)$$

Case II: Adaptive update of the spatial discretization of the coarse propagator for $k \geq 1$

We now introduce how to update the POD subspace adaptively which is used for the spatial discretization of the coarse propagator during each parareal iteration. The construction of the POD subspace used in the coarse propagator \mathcal{G}_0 only uses the snapshots obtained on $[0, T_0]$. The accuracy of the coarse propagator with this POD subspace for the spatial discretization is usually rather limited. As mentioned previously, we notice that during the parareal iterations, the propagation of the fine propagator on each time subinterval produces a large amount of data, which is in fact an approximation to the solution obtained by applying the fine propagator starting from the exact initial value with increasing accuracy during the iteration. Therefore, we consider to use the data to update the POD subspace. We believe that as the iteration proceeds, the accuracy of the coarse propagator using this updated POD subspace can approach to that of the fine propagator's spatial discretization progressively. We now introduce the details.

Let

$$T_0 = \hat{t}_0 < \hat{t}_1 < \hat{t}_2 < \dots < \hat{t}_n < \hat{t}_{n+1} < \dots < \hat{t}_N = T$$

be a partition of the time domain $[T_0, T]$. For simplicity, we still denote \hat{t}_n as t_n and the approximation of $u(t_n)$ at k -th parareal iteration as U_n^k in the remainder of this article. The solution obtained by the fine propagator at T_0 is denoted as \hat{u}_0 . Meanwhile, the solution obtained by applying the fine propagator starting from the exact initial value is denoted as U_n . We denote $\mathcal{G}_{k,n}$ the coarse propagator on the time subinterval $[t_n, t_{n+1}]$ during the k -th iteration, whose spatial discretization is carried out in the subspace $V_{n,POD}^k$. Our goal is to construct subspaces $\{V_{n,POD}^k\}_k$ such that the spatial discretization of the coarse propagator on these subspaces yields approximation with increasingly high accuracy as increasing k . From the data obtained by calculating $\mathcal{F}(t_n, t_{n+1}, U_n^{k-1})$, we collect the snapshots on each time subinterval in parallel. These snapshots can be used to construct new POD subspaces. In this way, we design an adaptive strategy, which fully utilizes data from previous iterations and adjacent time subintervals, to progressively refine the spatial discretization of the coarse propagator.

Now, we introduce the details. We first collect the numerical solutions per δM steps from calculating $\mathcal{F}(t_n, t_{n+1}, U_n^{k-1})$ to form the snapshot matrix $\mathbf{W}_{n,0}^k$. Then, choosing parameter $\gamma_2 \in (0, 1]$ and performing model reduction on $\mathbf{W}_{n,0}^k$ by POD_Mode $(\mathbf{W}_{n,0}^k, \gamma_2, \mathbf{M}, \Phi_h, m_{n,0}^k, \Psi_{n,0}^k, \tilde{\mathbf{R}}_{n,0}^k)$ as in Algorithm 1, we obtain new POD modes $\Psi_{n,0}^k$ on each time subinterval. For the time-dependent problems, the solution at this moment depends on the solution at the previous moment. We consider to utilize the data $\tilde{\mathbf{R}}_{n,0}^k$ from the previous p iterations and the left time subintervals to construct the POD subspace $\tilde{V}_{n,POD}^k$ on the time subinterval $[t_n, t_{n+1}]$ and obtain

$$\mathbf{W}_n^k = [\tilde{\mathbf{R}}_{n-m_l,0}^k, \tilde{\mathbf{R}}_{n-m_l+1,0}^k, \dots, \tilde{\mathbf{R}}_{n,0}^k, \tilde{\mathbf{R}}_{n,0}^{k-1}, \dots, \tilde{\mathbf{R}}_{n,0}^{k-p}], \quad (13)$$

where m_l denotes the number of time subintervals selected on the left side. Finally, choosing parameter $\gamma_3 \in (0, 1]$ and performing model reduction on \mathbf{W}_n^k by POD_Mode $(\mathbf{W}_n^k, \gamma_3, \mathbf{M}, \Phi_h, m_n^k, \Psi_n^k, \tilde{\mathbf{R}}_n^k)$ as in Algorithm 1, we obtain the POD subspace $\tilde{V}_{n,POD}^k$ spanned by POD modes Ψ_n^k on each subinterval.

We note that $U_n^k \notin \tilde{V}_{n,POD}^k$, which will introduce projection error when projecting the initial value onto the POD subspace during the sequential update of U_n^k . This part of the error can not be removed by updating the POD subspaces. To remove the errors introduced by the Galerkin projection, we improve our method by adding U_n^k to $\tilde{V}_{n,POD}^k$. The process is demonstrated in the following.

The POD modes for the n -th time subinterval in the k -th iteration are

$$\Psi_n^k = (\psi_{n,1}^k, \psi_{n,2}^k, \dots, \psi_{n,m_n^k}^k) = \Phi_h \tilde{\mathbf{R}}_n^k.$$

Denote $\mathbb{P}_{\tilde{V}_{n,POD}^k} : V_h \rightarrow \tilde{V}_{n,POD}^k$ the Galerkin projection onto the POD subspace $\tilde{V}_{n,POD}^k$. Considering $U_n^k = \Phi_h \mathbf{U}_n^k$, and denoting $\tilde{\mathbf{d}}_n^k$ the coefficient column vector of $U_n^k - \mathbb{P}_{\tilde{V}_{n,POD}^k}(U_n^k)$ in the basis Φ_h , we obtain

$$\tilde{\mathbf{d}}_n^k = \mathbf{U}_n^k - \tilde{\mathbf{R}}_n^k (\tilde{\mathbf{R}}_n^k)^\top \mathbf{M} \mathbf{U}_n^k. \quad (14)$$

Let $\mathbf{d}_n^k = \frac{\tilde{\mathbf{d}}_n^k}{\sqrt{(\tilde{\mathbf{d}}_n^k)^\top \mathbf{M} \tilde{\mathbf{d}}_n^k}}$, the new POD modes are

$$(\psi_{n,1}^k, \psi_{n,2}^k, \dots, \psi_{n,m_n^k+1}^k) = \Phi_h(\tilde{\mathbf{R}}_n^k, \mathbf{d}_n^k). \quad (15)$$

After adding U_n^k to $\tilde{V}_{n,\text{POD}}^k$, we obtain the final subspace $V_{n,\text{POD}}^k$. Set $\tilde{u}_{n,l}^k$ as the POD solution at $t = t_n + l \cdot dT$, $\tilde{u}_{n,l}^k = \sum_{i=1}^{m_n^k+1} \beta_{n,l,i}^k \psi_{n,i}^k$, and $\tilde{\mathbf{u}}_{n,l}^k = \left(\beta_{n,l,1}^k, \dots, \beta_{n,l,m_n^k+1}^k \right)^\top \cdot \mathbf{A}_{n,l}$ and $\mathbf{b}_{n,l}$ are the corresponding matrix and vector at $t_n + l \cdot dT$. By setting V_h in (7) to $V_{n,\text{POD}}^k$, we obtain

$$\left(\sum_{i=1}^{m_n^k+1} \beta_{n,l,i}^k \psi_{n,i}^k - \sum_{i=1}^{m_n^k+1} \beta_{n,l-1,i}^k \psi_{n,i}^k, \psi_{n,j}^k \right) + dT \cdot \left(\mathcal{A}(t_n + l \cdot dT, \sum_{i=1}^{m_n^k+1} \beta_{n,l,i}^k \psi_{n,i}^k), \psi_{n,j}^k \right) = 0.$$

Combining with (11), we can rewrite the equations above as

$$\begin{bmatrix} (\tilde{\mathbf{R}}_n^k)^\top \mathbf{A}_{n,l} \tilde{\mathbf{R}}_n^k & (\tilde{\mathbf{R}}_n^k)^\top \mathbf{A}_{n,l} \mathbf{d}_n^k \\ (\mathbf{d}_n^k)^\top \mathbf{A}_{n,l} (\tilde{\mathbf{R}}_n^k)^\top & (\mathbf{d}_n^k)^\top \mathbf{A}_{n,l} \mathbf{d}_n^k \end{bmatrix} \tilde{\mathbf{u}}_{n,l}^k = \begin{bmatrix} (\tilde{\mathbf{R}}_n^k)^\top \mathbf{b}_{n,l} \\ (\mathbf{d}_n^k)^\top \mathbf{b}_{n,l} \end{bmatrix} + \begin{bmatrix} (\tilde{\mathbf{R}}_n^k)^\top \mathbf{M} \tilde{\mathbf{R}}_n^k & (\tilde{\mathbf{R}}_n^k)^\top \mathbf{M} \mathbf{d}_n^k \\ (\mathbf{d}_n^k)^\top \mathbf{M} (\tilde{\mathbf{R}}_n^k)^\top & (\mathbf{d}_n^k)^\top \mathbf{M} \mathbf{d}_n^k \end{bmatrix} \tilde{\mathbf{u}}_{n,l-1}^k. \quad (16)$$

We then obtain our adaptive parareal method as the following formula (17):

$$\begin{cases} U_{n+1}^0 = \mathcal{G}_0(t_n, t_{n+1}, \mathbb{P}_{V_{n,\text{POD}}^0}(U_n^0)), & U_0^0 = \hat{u}_0, \\ U_{n+1}^k = \mathcal{G}_{k,n}(t_n, t_{n+1}, \mathbb{P}_{V_{n,\text{POD}}^k}(U_n^k)) + \mathcal{F}(t_n, t_{n+1}, U_n^{k-1}) - \mathcal{G}_{k,n}(t_n, t_{n+1}, \mathbb{P}_{V_{n,\text{POD}}^k}(U_n^{k-1})), & U_0^k = \hat{u}_0, \\ k = 1, 2, \dots \end{cases} \quad (17)$$

where $\mathcal{G}_{k,n}$ is the propagator whose spatial discretization is introduced above.

We summarize the general framework of the adaptive parareal method based on model order reduction as in Algorithm 2.

Algorithm 2 General framework of the adaptive parareal method based on model order reduction

- 1: Given the mesh \mathcal{T}_h , time steps $\delta t, dT$, parameters $\Delta T, \delta M, \gamma_1, \gamma_2, \gamma_3, p, m_l$;
- 2: Construct \mathcal{F} ;
- 3: Discretize (5) on $[0, T_0]$ by \mathcal{F} and obtain the snapshot matrix \mathbf{W}_h ;
- 4: Construct POD modes Ψ_h by `POD_Mode` $(\mathbf{W}_h, \gamma_1, \mathbf{M}, \Phi_h, m, \Psi_h, \tilde{\mathbf{R}})$ and obtain \mathcal{G}_0 ;
- 5: Discretize (5) on $[T_0, T]$ by \mathcal{G}_0 to obtain initial values U_n^0 for each time subinterval

$$U_0^0 = \hat{u}_0, \quad U_{n+1}^0 = \mathcal{G}_0(t_n, t_{n+1}, \mathbb{P}_{V_{n,\text{POD}}^0}(U_n^0)), n = 0, \dots, N-1;$$

- 6: $k = 1$;
- 7: **while** not converged **do**

```

8: Discretize (5) on  $[t_n, t_{n+1}]$  by  $\mathcal{F}$  in parallel to obtain  $\mathcal{F}(t_n, t_{n+1}, U_n^{k-1})$  and the
snapshot matrix  $\mathbf{W}_{n,0}^k, n = k-1, \dots, N-1$ ;
9: Construct  $\widetilde{\mathbf{R}}_{n,0}^k$  by POD_Mode  $(\mathbf{W}_{n,0}^k, \gamma_2, \mathbf{M}, \Phi_h, m_n^k, \Psi_n^k, \widetilde{\mathbf{R}}_{n,0}^k)$  and obtain

$$\mathbf{W}_n^k = [\widetilde{\mathbf{R}}_{n-m_l,0}^k, \widetilde{\mathbf{R}}_{n-m_l+1,0}^k, \dots, \widetilde{\mathbf{R}}_{n,0}^k, \widetilde{\mathbf{R}}_{n,0}^{k-1}, \dots, \widetilde{\mathbf{R}}_{n,0}^{k-p}],$$

in parallel,  $n = 0, \dots, N-1$ ;
10: Construct  $\widetilde{\mathbf{R}}_n^k$  by POD_Mode  $(\mathbf{W}_n^k, \gamma_3, \mathbf{M}, \Phi_h, m_n^k, \Psi_n^k, \widetilde{\mathbf{R}}_n^k)$  in parallel,
 $n = k-1, \dots, N-1$ ;
11:  $n = k$ ;
12: while  $n < N$  do
13:     Add  $U_n^k$  to the POD modes  $\Psi_n^k$  to get the final subspace  $V_{n,POD}^k$  and then
        obtain  $\mathcal{G}_{k,n}$ ;
14:     Discretize (5) on  $[t_n, t_{n+1}]$  by  $\mathcal{G}_{k,n}$  to obtain  $\mathcal{G}_{k,n}(t_n, t_{n+1}, \mathbb{P}_{V_{n,POD}^k}(U_n^{k-1}))$  and
         $\mathcal{G}_{k,n}(t_n, t_{n+1}, \mathbb{P}_{V_{n,POD}^k}(U_n^k))$  in parallel;
15:     Update  $U_{n+1}^k$  by

$$U_{n+1}^k = \mathcal{G}_{k,n}(t_n, t_{n+1}, \mathbb{P}_{V_{n,POD}^k}(U_n^k)) + \mathcal{F}(t_n, t_{n+1}, U_n^{k-1}) - \mathcal{G}_{k,n}(t_n, t_{n+1}, \mathbb{P}_{V_{n,POD}^k}(U_n^{k-1}));$$

16:     n++;
17: end while
18: k++.
19: end while

```

Remark 1. Compared with the plain parareal method, where $\mathcal{G}(t_n, t_{n+1}, U_n^{k-1})$ is obtained from the previous iteration, the addition of U_n^k to $\widetilde{V}_{n,POD}^k$ and the calculation of $\mathcal{G}_{k,n}(t_n, t_{n+1}, \mathbb{P}_{V_{n,POD}^k}(U_n^{k-1}))$ in our method must be done sequentially. Nonetheless, considering that the number of POD modes is significantly smaller than the dimension of the finite element space, and only one element is added, the additional computational cost remains little compared to that of the fine propagator.

3.3. Speed-up

It is known that the goal of a parareal method is to obtain high speed-up. In this subsection, we analyze the speed-up of our adaptive parareal method Algorithm 2.

We use the notation $\text{cost}_{\text{par}}([0, T])$ to denote the time cost of our adaptive parareal method Algorithm 2, and use notation $\text{cost}_{\text{seq}}([0, T])$ to denote the time cost for propagating the equation (1) by the fine propagator sequentially.

The speed-up is then defined as follows [19]

$$\text{speed-up}([0, T]) = \frac{\text{cost}_{\text{seq}}([0, T])}{\text{cost}_{\text{par}}([0, T])}.$$

We denote $\tau_{\mathcal{F}}$ and $\tau_{\mathcal{G}}$ the time cost for propagating the equation (1) one step by using the fine and coarse propagators respectively. Then we can deduce that the time cost $\text{cost}_{\text{seq}}([0, T])$ to carry the fine propagator serially is $(N \frac{\Delta T}{\delta t} + \frac{T_0}{\delta t})\tau_{\mathcal{F}}$. That is,

$$\text{cost}_{\text{seq}}([0, T]) = (N \frac{\Delta T}{\delta t} + \frac{T_0}{\delta t})\tau_{\mathcal{F}}.$$

We now analyze the cost for our adaptive parareal method Algorithm 2. The time cost for carrying the coarse propagator at the 0-th iteration is $N \frac{\Delta T}{dT} \tau_{\mathcal{G}}$. For each parareal iteration, the time cost for calculating $\mathcal{F}(t_n, t_{n+1}, U_n^{k-1})$ is $\frac{\Delta T}{\delta t} \tau_{\mathcal{F}}$. For the calculation of $\mathcal{G}_{k,n}(t_n, t_{n+1}, \mathbb{P}_{V_{n,\text{POD}}^k}(U_n^{k-1}))$ and $\mathcal{G}_{k,n}(t_n, t_{n+1}, \mathbb{P}_{V_{n,\text{POD}}^k}(U_n^k))$, since they are independent each other, they can be carried out in parallel essentially. Besides, considering that $U_k^k = U_k$, the coarse propagator does not have to execute from T_0 to T , but only needs to cover $[T_0 + k\Delta T, T]$. Therefore, the time cost is $(N - k)\frac{\Delta T}{dT} \tau_{\mathcal{G}}$. The time cost for obtaining or updating the coarse propagator, which only need to be carried once during each iteration, including constructing the POD subspace and obtaining the reduced system (11), is denoted as T_U . The time cost for adding U_n^k to the original POD subspace $\tilde{V}_{n,\text{POD}}^k$, which has to be carried in each time subinterval sequentially, is denoted as T_A . Denote k_{\max} the number of iterations.

Therefore, by the analysis above, we have that

$$\begin{aligned} \text{cost}_{\text{par}}([0, T]) &= \frac{T_0}{\delta t} \tau_{\mathcal{F}} + T_U + N \frac{\Delta T}{dT} \tau_{\mathcal{G}} + \sum_{k=1}^{k_{\max}} \left(\frac{\Delta T}{\delta t} \tau_{\mathcal{F}} + T_U + (N - k) \left(T_A + \frac{\Delta T}{dT} \tau_{\mathcal{G}} \right) \right) \\ &= \frac{T_0}{\delta t} \tau_{\mathcal{F}} + T_U + N \frac{\Delta T}{dT} \tau_{\mathcal{G}} + k_{\max} \left(\frac{\Delta T}{\delta t} \tau_{\mathcal{F}} + T_U + \left(N - \frac{k_{\max} + 1}{2} \right) \left(T_A + \frac{\Delta T}{dT} \tau_{\mathcal{G}} \right) \right). \end{aligned}$$

In further, we analyze the cost for each part.

We first analyze $\tau_{\mathcal{F}}$. Due to the sparsity of the matrices in the linear system (10), the computational complexity for constructing (10) is $C_{f_1} N_g$ [14], with the constant factor C_{f_1} depending on the type of finite element, which is usually of magnitude tens or hundreds. For solving the linear system (10), although there exist some linear solvers which can achieve approximately linear complexity, their constant factors are highly problem-dependent and typically very large, often being of magnitude hundreds or thousands. Therefore, $\tau_{\mathcal{F}} \approx C_{f_1} N_g + C_{f_2} N_g$, with C_{f_1} being of magnitude tens or hundreds and C_{f_2} being of magnitude hundreds or thousands.

Furthermore, for the cases where $\mathcal{A}(t, u)$ can be separable in time and space, we only need to construct the system (10) at the first time step. Therefore, in this case, $\tau_{\mathcal{F}} \approx C_{f_2} N_g$.

For simplicity, we write $\tau_{\mathcal{F}} \approx C_f N_g$ with $C_f = C_{f_1} + C_{f_2}$ or $C_f = C_{f_2}$, a constant being of magnitude hundreds or thousands.

We then analyze $\tau_{\mathcal{G}}$. Denote m_{\max} the maximum dimension of the POD subspaces across all time subintervals. For solving the the reduced system (11), whose coefficient matrix is dense, we know that the computational complexity is $C_{p_1} m_{\max}^3$, where C_{p_1} can be less than 1. Hence, $\tau_{\mathcal{G}} \approx C_{p_1} m_{\max}^3$.

For the time cost T_U , it contains two cases. For the 0-th iteration, the computational complexity of performing model order reduction operation on \mathbf{W}_h is about

$C_{p_2}n_s^2N_g$ [26], where $n_s = \left\lfloor \frac{\Delta T}{\delta t \cdot \delta M} \right\rfloor + 1$, and the constant factor C_{p_2} can be less than 10. Once we obtain the POD subspace, the time cost for obtaining the reduced system (11) is $C_{p_3}m_{\max}^2N_g$, with constant factor C_{p_3} usually being of magnitude tens. So $T_U \approx C_{p_2}n_s^2N_g + C_{p_3}m_{\max}^2N_g$. For the k -th iteration with $k \geq 1$, the operation of model order reduction has to be carried out twice. The first is performed on $\mathbf{W}_{n,0}^k$, and the second is on \mathbf{W}_n^k . Let n_{\max} be the maximum column dimension of the matrices involved in the SVD across all time subintervals. Then, we have $T_U \approx C_{p_2}(n_s^2 + n_{\max}^2)N_g + C_{p_3}m_{\max}^2N_g$.

Finally, similar to the cost for obtaining the system (11), we can see that the cost for calculating (14) is about $C_{p_3}m_{\max}N_g$, that is, $T_A \approx C_{p_3}m_{\max}N_g$.

Therefore, for the case where $\mathcal{A}(t, u)$ can be separable in time and space, we have

$$\begin{aligned} \text{cost}_{\text{par}}([0, T]) &= \frac{T_0}{\delta t} \tau_{\mathcal{F}} + T_U + N \frac{\Delta T}{dT} \tau_{\mathcal{G}} + k_{\max} \left(\frac{\Delta T}{\delta t} \tau_{\mathcal{F}} + T_U + \left(N - \frac{k_{\max} + 1}{2} \right) \left(T_A + \frac{\Delta T}{dT} \tau_{\mathcal{G}} \right) \right) \\ &= \frac{T_0}{\delta t} C_f N_g + C_{p_2} n_s^2 N_g + C_{p_3} m_{\max}^2 N_g + C_{p_1} N \frac{\Delta T}{dT} m_{\max}^3 \\ &\quad + k_{\max} \left(\frac{\Delta T}{\delta t} C_f N_g + C_{p_2} (n_s^2 + n_{\max}^2) N_g + C_{p_3} m_{\max}^2 N_g + \left(N - \frac{k_{\max} + 1}{2} \right) \left(C_{p_3} m_{\max} N_g + \frac{\Delta T}{dT} C_{p_1} m_{\max}^3 \right) \right) \\ &= \left(\frac{T_0}{\delta t} C_f + C_{p_2} n_s^2 + C_{p_3} m_{\max}^2 + k_{\max} \left(\frac{\Delta T}{\delta t} C_f + C_{p_2} (n_s^2 + n_{\max}^2) + C_{p_3} m_{\max}^2 + C_{p_3} m_{\max} \left(N - \frac{k_{\max} + 1}{2} \right) \right) \right) N_g \\ &\quad + C_{p_1} \frac{\Delta T}{dT} \left(N + k_{\max} \left(N - \frac{k_{\max} + 1}{2} \right) \right) m_{\max}^3, \end{aligned}$$

and

$$\text{cost}_{\text{seq}}([0, T]) = \left(N \frac{\Delta T}{\delta t} + \frac{T_0}{\delta t} \right) \tau_{\mathcal{F}} = \left(N \frac{\Delta T}{\delta t} + \frac{T_0}{\delta t} \right) C_f N_g.$$

From the former analysis, we know that C_f is usually of magnitude hundreds or thousands, while C_{p_1} is usually less than 1, C_{p_2} and C_{p_3} are usually of magnitude tens. Besides, from our numerical tests, we know that m_{\max} , n_s , and n_{\max} generally do not exceed an order of magnitude of a hundred. Note that $\Delta T \gg \delta t$ and $N_g \gg m_{\max}^3$, we have that $C_{p_2}(n_s^2 + n_{\max}^2) + C_{p_3}m_{\max}^2 \leq \frac{\Delta T}{\delta t}$. For the convenience of our analysis for the speedup, we only keep the dominate term in the $\text{cost}_{\text{par}}([0, T])$. That is, we have

$$\text{cost}_{\text{par}}([0, T]) \approx \left(\frac{T_0}{\delta t} C_f + k_{\max} \left(\frac{\Delta T}{\delta t} C_f + C_{p_3} m_{\max} \left(N - \frac{k_{\max} + 1}{2} \right) \right) \right) N_g.$$

Assume that we have N processors, that is, the number of processors is equal to the number of time subinterval, and each processor deals with one time subinterval. If we ignore the communication time and only keep the dominate term in the $\text{cost}_{\text{par}}([0, T])$,

we have that

$$\begin{aligned}
\text{speed-up}([0, T]) &= \frac{\text{cost}_{\text{seq}}([0, T])}{\text{cost}_{\text{par}}([0, T])} \\
&\approx \frac{\left(N \frac{\Delta T}{\delta t} + \frac{T_0}{\delta t}\right) C_f N_g}{\left(\frac{T_0}{\delta t} C_f + k_{\max} \left(\frac{\Delta T}{\delta t} C_f + C_{p_3} m_{\max} \left(N - \frac{k_{\max}+1}{2}\right)\right)\right) N_g} \\
&= \frac{\left(N \frac{\Delta T}{\delta t} + \frac{T_0}{\delta t}\right) C_f}{\frac{T_0}{\delta t} C_f + k_{\max} \left(\frac{\Delta T}{\delta t} C_f + C_{p_3} m_{\max} \left(N - \frac{k_{\max}+1}{2}\right)\right)} \\
&\approx \min\left(\frac{N}{k_{\max}}, \frac{\Delta T}{\delta t} \frac{C_f}{C_{p_3} m_{\max}}\right).
\end{aligned}$$

Note that from the former analysis, we usually have $C_f \geq C_{p_3} m_{\max}$. Therefore, we can see that, for fixed ΔT and δt with $\Delta T \gg \delta t$, if k_{\max} is not too large, we can see that the larger N , the higher speedup we will obtain, until some maximum speedup is obtained. For fixed ΔT , the larger N means the larger T . Therefore, by our adaptive parareal method, we can obtain very large speedup for long time simulation, if we have enough number of processors.

4. Numerical experiments

We consider the following time-dependent partial differential equations with periodic boundary conditions

$$\begin{cases} u_t - \epsilon \Delta u + \mathbf{B}(x, y, z, t) \cdot \nabla u + c(x, y, z, t)u = f(x, y, z, t), & \text{in } \Omega \times (0, T], \\ u(x, y, z, 0) = h(x, y, z), & \text{in } \Omega \\ u(x + L, y, z, t) = u(x, y + L, z, t) = u(x, y, z + L, t) = u(x, y, z, t), & \text{on } \partial\Omega \times (0, T], \end{cases} \quad (18)$$

where $\Omega = [0, L]^3$, $f \in L^2(0, T; L^2(\Omega))$, $c \in C(0, T; L^\infty(\Omega))$, $\mathbf{B} \in C(0, T; W^{1,\infty}(\Omega)^3)$, $h \in L^2(\Omega)$ and ϵ is a positive constant. Generally, the smaller the ϵ , the more challenging the simulation of this model becomes.

In our numerical simulation, we choose two typical fluid advection fields in three dimensional space to show the performance of our methods. The relative error of approximation U_n^k at $t = t_n$ obtained by our parareal method is calculated by

$$\text{Error} = \frac{\|U_n^k - U_n\|_{L^2}}{\|U_n\|_{L^2}}, \quad (19)$$

where the reference solution U_n is that obtained by propagating (18) using the fine propagator with exact initial values over $[0, T]$.

In the following discussions, we denote our adaptive parareal method Algorithm 2 as ‘‘AdapParareal’’. For the method ‘‘AdapParareal’’, we test the following 4 cases respectively: $(m_l, p) = (0, 0), (1, 0), (0, 1), (1, 1)$. For the sake of simplicity, we denote $\mathcal{G}_{k,n}(t_n, t_{n+1}, \mathbb{P}_{V_{n,\text{POD}}}^k(U_n^k))$ as $\mathcal{G}_k(U_n^k)$ in this section. For comparison, we have also done some tests using the plain parareal method, in which the coarse propagator is spatially

discretized by the POD method without any subspace updating. This approach is denoted as “Parareal”.

Our numerical experiments are carried out on the high performance computers of State Key Laboratory of Mathematical Sciences, Chinese Academy of Sciences, and our code is based on the toolbox PHG [1]. It should be noted that, due to the limitation of computational resources, the steps 8-10 and the step 14 in Algorithm 2 which should be executed in essentially parallel across time subintervals are instead carried out sequentially, one time subinterval at a time.

4.1. Kolmogorov flow

We consider the advection-diffusion equation (18), where the advection field is defined by the Kolmogorov flow [8, 36]. The components of the equation are given as follows:

$$\begin{aligned}\mathbf{B}(x, y, z, t) &= (\cos(y), \cos(z), \cos(x)) + (\sin(z), \sin(x), \sin(y)) \cos(t), \\ f(x, y, z, t) &= -\cos(y) - \sin(z) \cos(t), \\ c(x, y, z, t) &= 0, \quad h(x, y, z) = 0, \quad L = 2\pi, \quad T = 1005.0.\end{aligned}\tag{20}$$

In this example, \mathbf{B} and f are separable in time and space, so the computation for constructing the discretized system can be simplified. We refer to [14] for more details. We use piecewise linear functions as the basis functions for the finite element method. We first divide Ω into 6 tetrahedrons to create the initial grid and refine the initial mesh 21 times uniformly using bisection to obtain the final mesh. The number of degrees of freedom is 2097152. We fix the parameters $\delta t = 1 \times 10^{-2}$, $dT = 0.5$, $\Delta T = T_0 = 5.0$, $\delta M = 5$, $\gamma_1 = \gamma_2 = 1.0 - 5.0 \times 10^{-6}$ and $\gamma_3 = 1.0 - 2.0 \times 10^{-8}$. The number of time subintervals is 200. For all figures in this article, the x -axis represents time t and k represents the index of iteration the y -axis represents the relative error of U_n^k defined by (19).

For comparison, we first test the two cases with $\epsilon = 0.5$ and 0.1 by using the method “Parareal”. Here, we set $T_0 = 10.0$. For fairness in comparison, we set the other parameters to be the same as those used in the method “AdapParareal”. The numerical results are shown in Fig. 1. The dimensions of POD subspaces for the coarse propagator in the 0-th iteration for these two cases are 24 and 38, respectively. For problem (18)-(20), we know that the smaller the ϵ , the more rapidly varies the solution. That’s the reason for the difference between number of POD modes obtained. From the two sub-figures in Fig. 1, we can see that the relative error can reach $O(10^{-3})$ after several iterations. It shows the effectiveness of method “Parareal”. However, we also see that the accuracy can not be improved any more as the increase of iteration. Considering that the model will be more difficult to be simulated as ϵ decreases, we can not expect better results for smaller ϵ and hence skip the showing of the numerical results for cases of smaller ϵ .

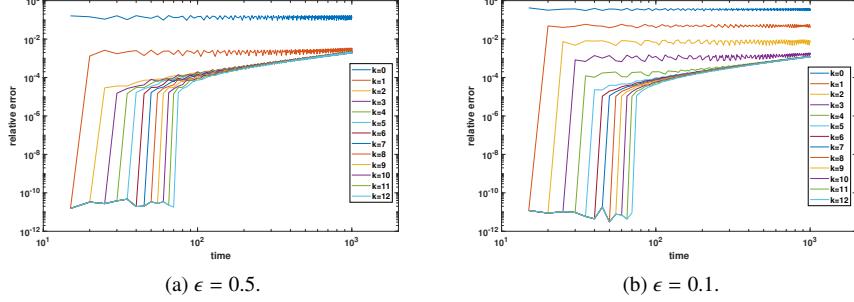


Figure 1: The evolution curves of the relative error of U_n^k obtained by the method ‘‘Parareal’’ in each parareal iteration for solving the Kolmogorov flow with $\epsilon = 0.5, 0.1$

We then use these two cases with $\epsilon = 0.5$ and 0.1 to show the performance of our new method ‘‘AdapParareal’’ with different (m_l, p) . The dimensions of POD subspaces for the coarse propagator in the 0-th iteration are 15 and 20 respectively. The corresponding results are presented in Fig. 2-5. First, from these figures, it is easy to see that the relative error can reach at least $O(10^{-3})$ after several iterations. This indicates that our adaptive parareal method is effective. Besides, by comparing them with Fig. 1, we find that our adaptive parareal method has better performance than that of the method ‘‘Parareal’’ in achieving high accuracy. For the cases of $(m_l, p) = (1, 0), (1, 1)$, the accuracy can reach even $O(10^{-10})$ after several iterations. Furthermore, the relative error does not increase rapidly over time, which indicates that our adaptive parareal method can perform well for simulating long-term evolution.

By comparing the numerical results using different (m_l, p) in Fig. 2-5, we observe that as the number of time subintervals used in constructing the coarse propagator increases, the convergence becomes faster. However, selecting more time subintervals will increase the number of POD modes, thereby increasing the computational cost.

Motivated by the above observations, when turning to the more challenging advection-dominated problems with $\epsilon = 0.05, 0.01, 0.005$, we adopt the setting $(m_l, p) = (1, 1)$. The corresponding numerical results are reported in Fig. 6. The dimensions of the POD subspaces for the coarse propagator in the 0-th iteration for these three cases are 24, 32, and 35, respectively.

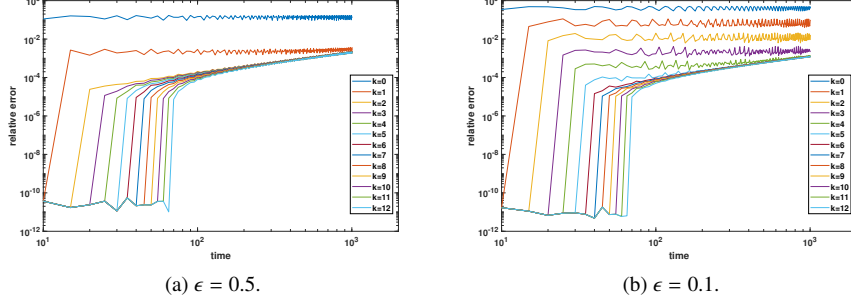


Figure 2: The evolution curves of the relative error of U_n^k obtained by the method ‘‘AdapParareal’’ in each parareal iteration for solving the Kolmogorov flow with $(m_l, p) = (0, 0)$ and $\epsilon = 0.5, 0.1$

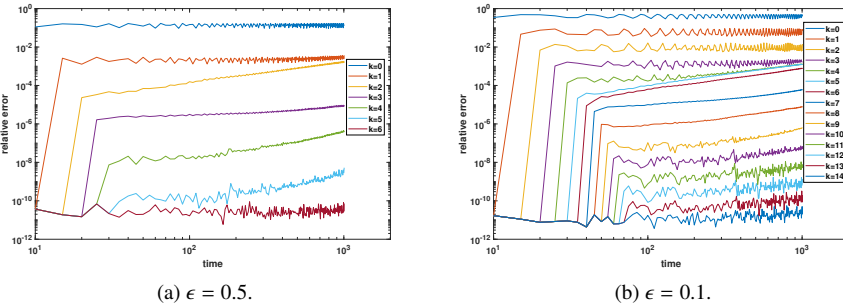


Figure 3: The evolution curves of the relative error of U_n^k obtained by the method ‘‘AdapParareal’’ in each parareal iteration for solving the Kolmogorov flow with $(m_l, p) = (1, 0)$ and $\epsilon = 0.5, 0.1$

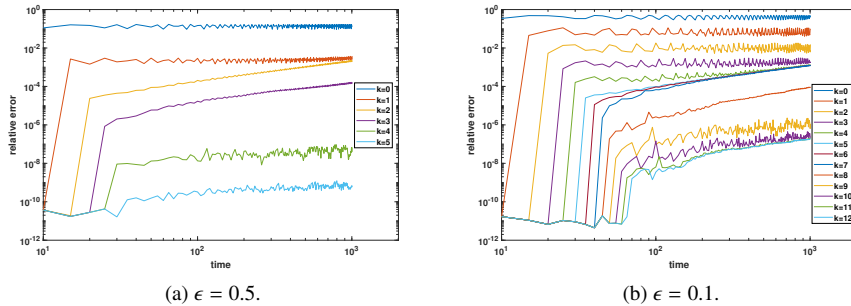


Figure 4: The evolution curves of the relative error of U_n^k obtained by the method ‘‘AdapParareal’’ in each parareal iteration for solving the Kolmogorov flow with $(m_l, p) = (0, 1)$ and $\epsilon = 0.5, 0.1$

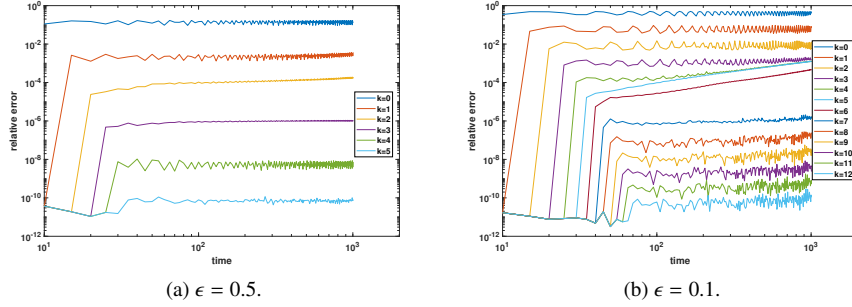


Figure 5: The evolution curves of the relative error of U_n^k obtained by the method ‘‘AdapParareal’’ in each parareal iteration for solving the Kolmogorov flow with $(m_l, p) = (1, 1)$ and $\epsilon = 0.5, 0.1$

From Fig. 6, we can first see that, as the parareal iteration continues, the error decreases obviously. However, compared with the cases $\epsilon = 0.5$ and $\epsilon = 0.1$, the convergence of the adaptive parareal method for these cases is slower. The reason lies in the fact that the smaller ϵ , the more difficult to be simulated. Fortunately, after several iterations, the accuracy obtained by our adaptive parareal method can be very high in long-term evolution. In fact, we can see that even for the case of $\epsilon = 0.005$, which is very difficult to be simulated well, after 24 parareal iterations, the error obtained on the whole time interval can be smaller than 2×10^{-6} .

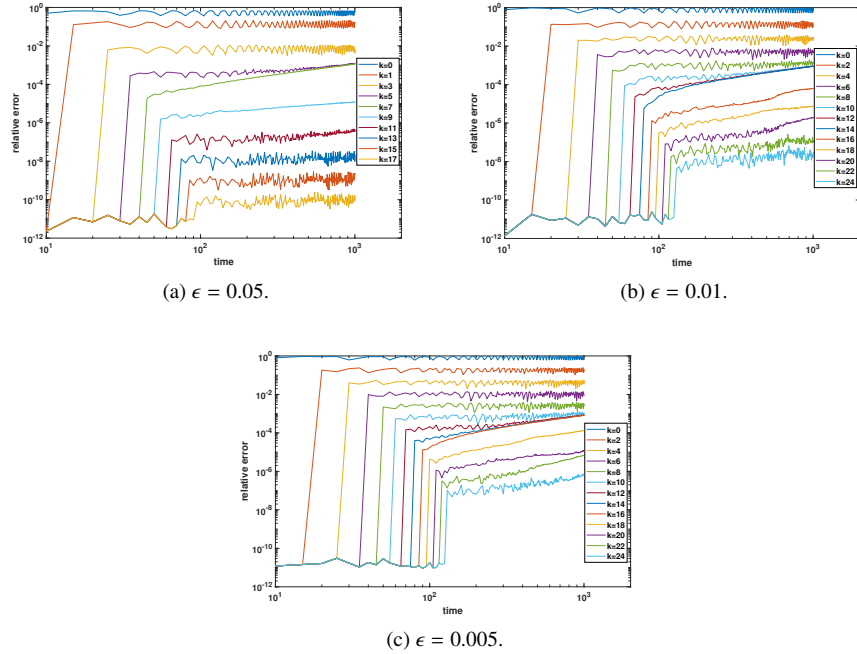


Figure 6: The evolution curves of the relative error of U_n^k obtained by the method ‘‘AdapParareal’’ in each parareal iteration for solving the Kolmogorov flow with $(m_l, p) = (1, 1)$ and $\epsilon = 0.05, 0.01, 0.005$

In the introduction part, we state that we believe that as the iteration proceeds, the spatial discretization accuracy of the coarse propagator will approach to that of the fine propagator's spatial discretization progressively. We want to point out that we have also done some tests to demonstrate it. Here, to remove the impact of the temporal discretization, we choose to use the same temporal discretization scheme and time step size used in the fine propagator. That is, the only difference between fine and coarse propagator lies in the spacial discretization, one discretizes the problem in the finite element space, the other discretizes the problem in the adaptive POD subspace. That is, we set $dT = \delta t = 0.01$. To see the performance, we show the difference between the approximation obtained with the coarse propagator and the fine propagator starting from the same initial values and the relative error of $\mathcal{G}_k(U_{n-1}^k)$, that is, we show $\frac{\|\mathcal{F}(U_{n-1}^{k-1}) - \mathcal{G}_k(U_{n-1}^{k-1})\|_{L^2}}{\|\mathcal{F}(U_{n-1}^{k-1})\|_{L^2}}$ and $\frac{\|U_n - \mathcal{G}_k(U_{n-1}^k)\|_{L^2}}{\|U_n\|_{L^2}}$. The numerical results for the Kolmogorov flow with $\epsilon = 0.05, 0.01, 0.005$ respectively are presented in Fig. 7-8. First, from these figures, we find that $\frac{\|\mathcal{F}(U_{n-1}^{k-1}) - \mathcal{G}_k(U_{n-1}^{k-1})\|_{L^2}}{\|\mathcal{F}(U_{n-1}^{k-1})\|_{L^2}}$ can reach at least $O(10^{-4})$ for all subintervals and iterations, which indicates that the accuracy of the term $\mathcal{G}_k(U_{n-1}^{k-1})$ is very high. Furthermore, from these sub-figures, we observe that as the increase of the parareal iteration, the accuracy of the coarse propagator improves obviously. After several times of iteration, the accuracy of the coarse propagator becomes very high. This shows that as the parareal iteration proceeds, the accuracy of spatial discretization of the coarse propagator can indeed be improved. From these tests, we can see that our adaptive parareal method can also be viewed as a parareal based adaptive POD method, which uses data obtained by fine propagator in each time subinterval during the parareal iteration to update the POD subspace adaptively. By using the idea of parareal method, for this adaptive parareal adaptive POD method, the update of the POD subspace for each time subinterval can be carried out essentially parallel. As the iteration continues, the accuracy of the POD method improves obviously.

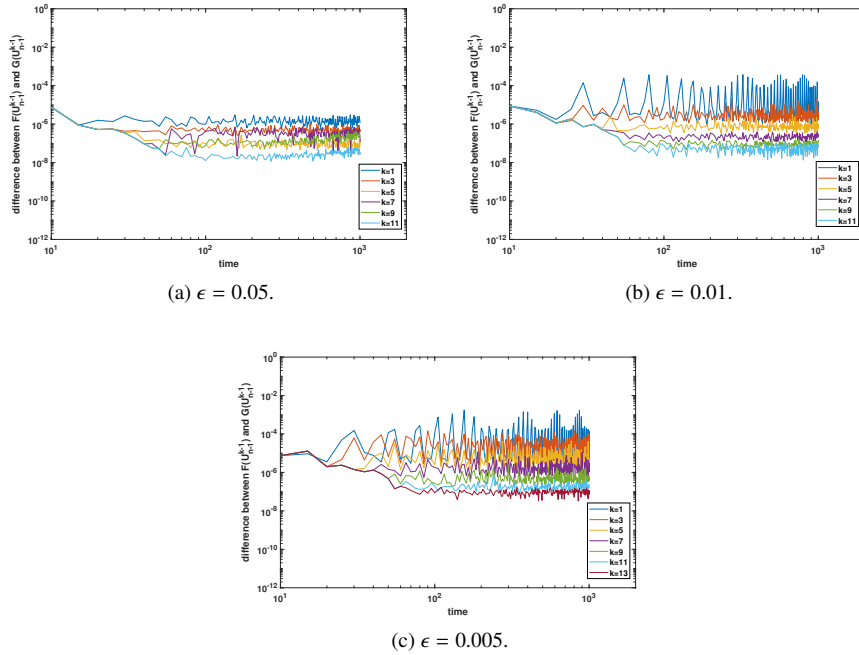


Figure 7: The evolution curves of $\frac{\|\mathcal{F}(U_{n-1}^{k-1}) - \mathcal{G}_k(U_{n-1}^{k-1})\|_{L^2}}{\|\mathcal{F}(U_{n-1}^{k-1})\|_{L^2}}$ obtained by the method ‘‘AdapParareal’’ in each parareal iteration for solving the Kolmogorov flow with $(m_l, p) = (1, 1)$ and $\epsilon = 0.05, 0.01, 0.005$

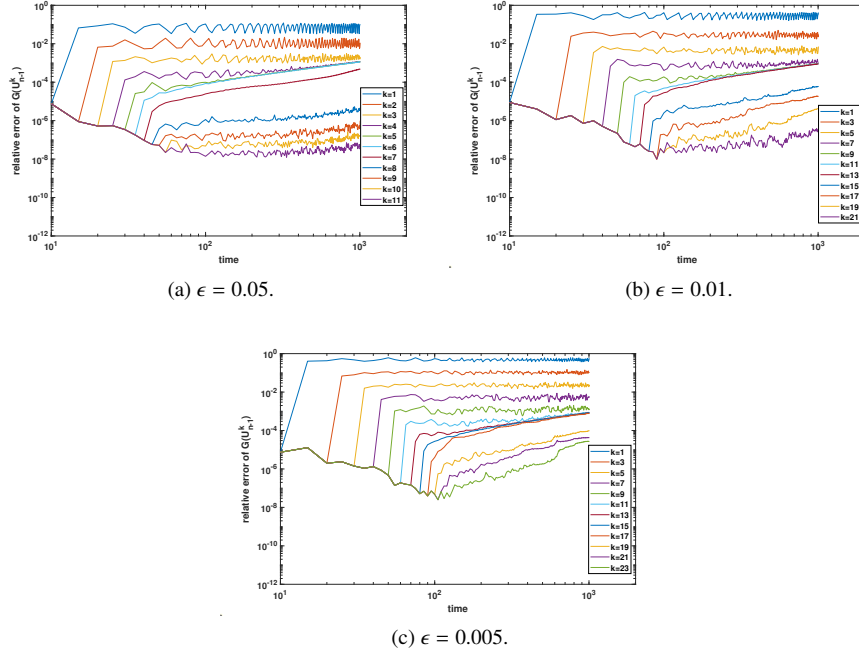


Figure 8: The evolution curves of $\frac{\|U_n - \mathcal{G}_k(U_{n-1}^k)\|_{L^2}}{\|U_n\|_{L^2}}$ obtained by the method ‘‘AdapParareal’’ in each parareal iteration for solving the Kolmogorov flow with $(m_l, p) = (1, 1)$ and $\epsilon = 0.05, 0.01, 0.005$

4.2. Arnold-Belt-Childress (ABC) flow

We then consider the advection-diffusion equation (18) where the advection field is defined by the Arnold-Belt-Childress (ABC) flow [10, 43]. The components of the equation are given as follows:

$$\begin{aligned}\mathbf{B}(x, y, z, t) &= (\sin(z + \sin wt) + \cos(y + \sin wt), \sin(x + \sin wt) \\ &\quad + \cos(z + \sin wt), \sin(y + \sin wt) + \cos(x + \sin wt)), \\ f(x, y, z, t) &= -\sin(z + \sin wt) - \cos(y + \sin wt), \\ c(x, y, z, t) &= 0, h(x, y, z) = 0, L = 2\pi, w = 1.0, T = 1005.0.\end{aligned}\tag{21}$$

In this example, \mathbf{B} and f are also separable in time and space. We also use piecewise linear functions as the basis functions for the finite element method. We first divide Ω into 6 tetrahedrons to create the initial grid and refine the initial mesh 21 times uniformly using bisection to obtain the final mesh. The number of degrees of freedom is 2097152. We fix the parameters $\delta t = 1 \times 10^{-2}$, $dT = 0.5$, $\Delta T = T_0 = 5.0$, $\delta M = 5$, $\gamma_1 = \gamma_2 = 1.0 - 5.0 \times 10^{-6}$ and $\gamma_3 = 1.0 - 2.0 \times 10^{-8}$. The number of time subintervals is also set to 200.

Similar to the case for the Kolmogorov flow, we first also test the two cases with $\epsilon = 0.5$ and 0.1 by the method ‘‘Parareal’’. Here, we also set $T_0 = 10.0$. Other parameters are the same as those in the method ‘‘AdapParareal’’. The numerical results are shown in Fig. 9. The dimensions of POD subspaces for the coarse propagator in the 0-th iteration for these two cases are 30 and 46 respectively. From the two sub-figures in Fig. 9, we can also see that the relative error can reach $O(10^{-3})$ after several iterations, which also indicates the effectiveness of the model order reduction based parareal method. Similar to the first example, the accuracy can not be improved any more as the increase of iteration.

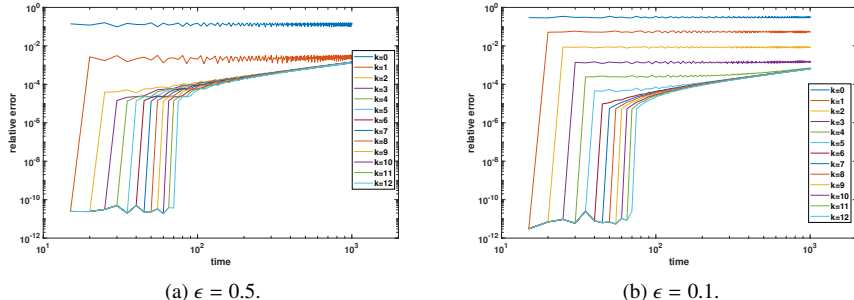


Figure 9: The evolution curves of the relative error of U_n^k obtained by the method ‘‘Parareal’’ in each parareal iteration for solving the ABC flow with $\epsilon = 0.5, 0.1$

Then, we also use these two cases with $\epsilon = 0.5$ and 0.1 to show the performance of our new method ‘‘AdapParareal’’ with different (m_l, p) . The dimensions of POD subspaces obtained for the coarse propagator in the 0-th iteration are 18 and 24 respectively. The corresponding results are presented in Fig. 10-13. Similar to the example of

the Kolmogorov flow, we can see that the relative error can reach at least $O(10^{-3})$ after several iterations from these figures, which also shows that the method “AdapParareal” is effective. Besides, when comparing them with the method “Parareal” in Fig. 9, the numerical results show that higher accuracy can be obtained by the method “AdapParareal”. Similarly, the relative error does not increase rapidly over time, which means that our adaptive parareal method has good performance for simulating long-term evolution.

Similar to the first example, by comparing the numerical results using different (m_l, p) in Fig. 10-13, we also observe that as the number of time subintervals used in constructing the coarse propagator increases, the convergence becomes faster. Meanwhile, the accuracy can also be improved to $O(10^{-10})$ for the case of $(m_l, p) = (1, 0)$, $(1, 1)$. However, selecting more time subintervals will increase the number of POD modes and the computational cost.

When we simulate the advection-dominated cases with $\epsilon = 0.05, 0.01, 0.005$ by the method “AdapParareal”, we also choose the best case of $(m_l, p) = (1, 1)$. The numerical results are presented in Fig. 14. The dimensions of POD subspaces for the initial coarse propagator in the 0-th iteration are 28, 40 and 44 respectively.

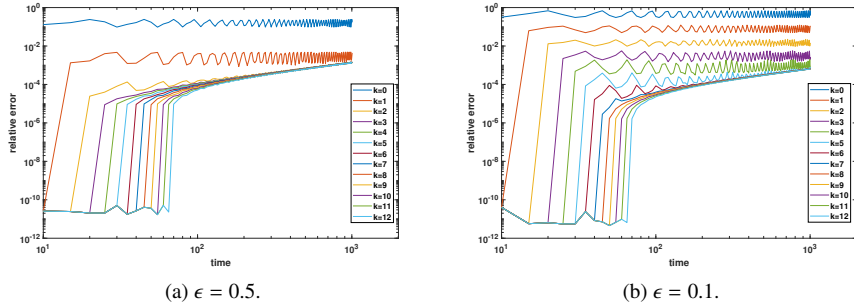


Figure 10: The evolution curves of the relative error of U_n^k obtained by the method “AdapParareal” in each parareal iteration for solving the ABC flow with $(m_l, p) = (0, 0)$ and $\epsilon = 0.5, 0.1$

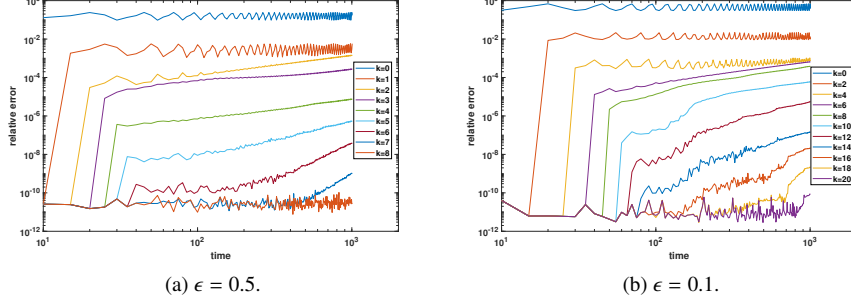


Figure 11: The evolution curves of the relative error of U_n^k obtained by the method “AdapParareal” in each parareal iteration for solving the ABC flow with $(m_l, p) = (1, 0)$ and $\epsilon = 0.5, 0.1$

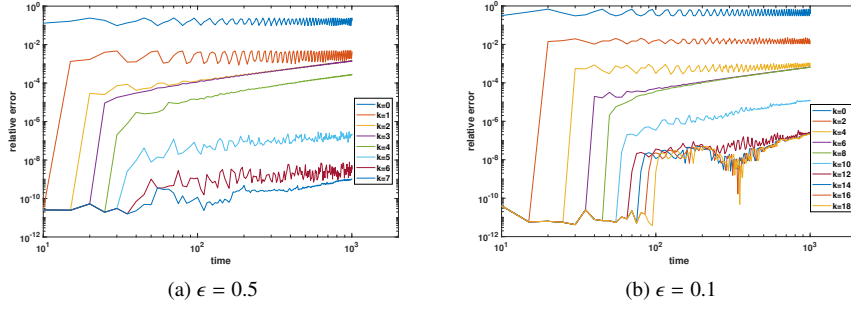


Figure 12: The evolution curves of the relative error of U_n^k obtained by the method “AdapParareal” in each parareal iteration for solving the ABC flow with $(m_l, p) = (0, 1)$ and $\epsilon = 0.5, 0.1$

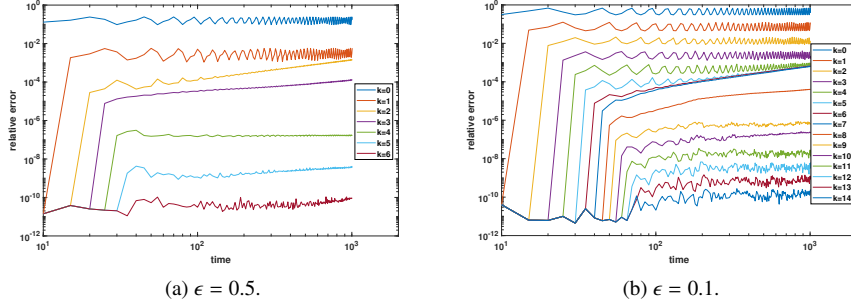


Figure 13: The evolution curves of the relative error of U_n^k obtained by the method “AdapParareal” in each parareal iteration for solving the ABC flow with $(m_l, p) = (1, 1)$ and $\epsilon = 0.5, 0.1$

Similar to the case of the Kolmogorov flow, we can also see from Fig. 14 that, the

error decreases obviously as the parareal iteration continues. However, compared with the cases $\epsilon = 0.5$ and $\epsilon = 0.1$, the convergence of the adaptive parareal method for these three cases is slower. Fortunately, the accuracy obtained by our adaptive parareal method can still be very high in long-term evolution after several iterations. We can also see that even for the case of $\epsilon = 0.005$, after 24 parareal iterations, the error obtained on the whole time interval can be smaller than 2×10^{-5} .

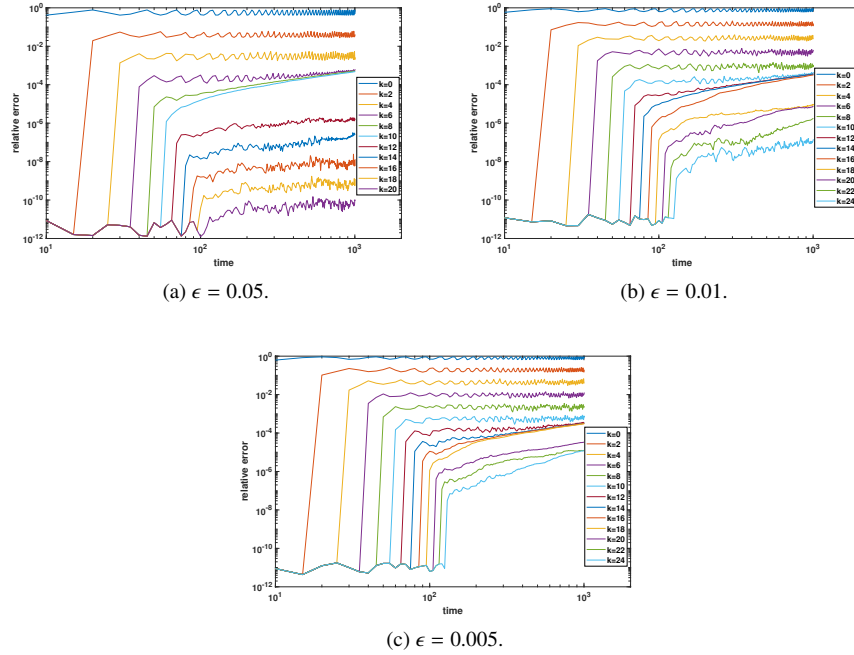


Figure 14: The evolution curves of the relative error of U_n^k obtained by the method “AdapParareal” in each parareal iteration for solving the ABC flow with $(m_l, p) = (1, 1)$ and $\epsilon = 0.05, 0.01, 0.005$

Similar to the first example, we have also done some tests to demonstrate that the spatial discretization accuracy of the coarse propagator will approach to that of the fine propagator's spatial discretization progressively as the iteration proceeds. We also set $dT = \delta t = 0.01$ to remove the impact of the temporal discretization. We show the difference between the approximation obtained with the coarse propagator and the fine propagator starting from the same initial values and the relative error of $\mathcal{G}_k(U_{n-1}^k)$, that is $\frac{\|\mathcal{F}(U_{n-1}^{k-1}) - \mathcal{G}_k(U_{n-1}^{k-1})\|_{L^2}}{\|\mathcal{F}(U_{n-1}^{k-1})\|_{L^2}}$ and $\frac{\|U_n - \mathcal{G}_k(U_{n-1}^k)\|_{L^2}}{\|U_n\|_{L^2}}$. The numerical results of the ABC flow with $\epsilon = 0.05, 0.01, 0.005$ respectively are presented in Fig. 15-16. From these figures, we can first see that $\frac{\|\mathcal{F}(U_{n-1}^{k-1}) - \mathcal{G}_k(U_{n-1}^{k-1})\|_{L^2}}{\|\mathcal{F}(U_{n-1}^{k-1})\|_{L^2}}$ can reach at least $O(10^{-4})$ for all subintervals and iterations, which indicates that the accuracy of the term $\mathcal{G}_k(U_{n-1}^{k-1})$ is very high. Moreover, we also observe that as the increase of the parareal iteration, the accuracy of the coarse propagator improves obviously. After several times of iteration, the accuracy of

the coarse propagator becomes very high. This also shows that as the parareal iteration proceeds, the accuracy of spatial discretization of the coarse propagator can indeed be improved. Therefore, similar to the first example, our adaptive parareal method can also be viewed as a parareal based adaptive POD method.

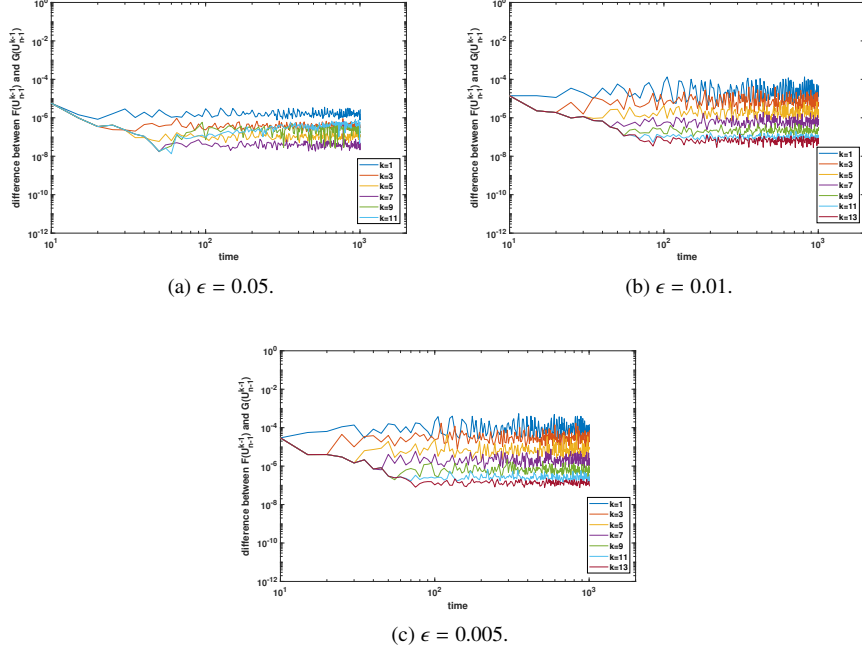


Figure 15: The evolution curves of $\frac{\|\mathcal{F}(U_{n-1}^{k-1}) - \mathcal{G}_k(U_{n-1}^{k-1})\|_{L^2}}{\|\mathcal{F}(U_{n-1}^{k-1})\|_{L^2}}$ obtained by the method “AdapParareal” in each parareal iteration for solving the ABC flow with $(m_l, p) = (1, 1)$ and $\epsilon = 0.05, 0.01, 0.005$

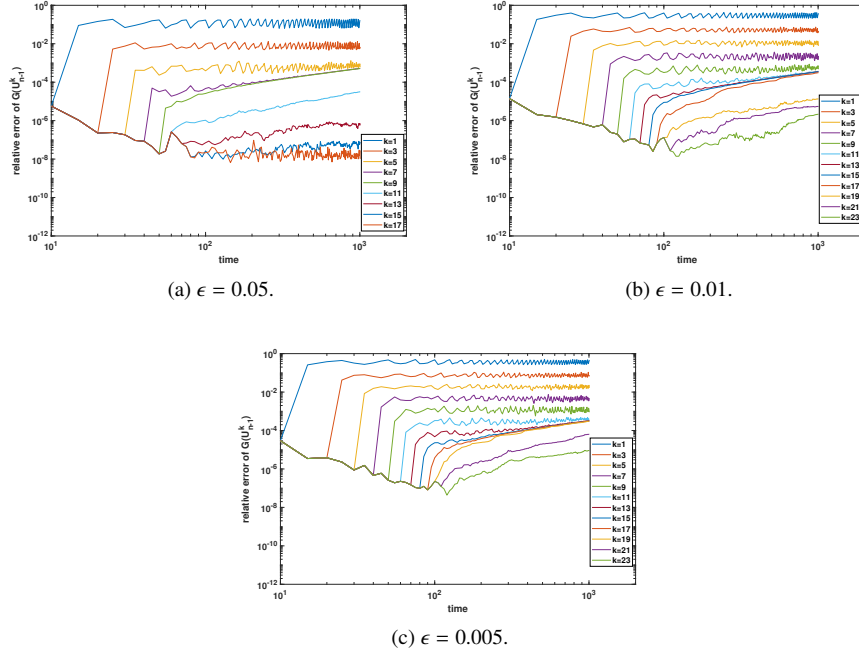


Figure 16: The evolution curves of $\frac{\|U_n - \mathcal{G}_k(U_{n-1}^k)\|_{L2}}{\|U_n\|_{L2}}$ obtained by the method ‘‘AdapParareal’’ in each parareal iteration for solving the ABC flow with $(m_l, p) = (1, 1)$ and $\epsilon = 0.05, 0.01, 0.005$

5. Concluding remarks

In this paper, we have proposed a model order reduction based adaptive parareal method for time-dependent partial differential equations. The main feature of our new method is that it updates the spatial discretization of the coarse propagator adaptively using data obtained by the fine propagator at each iteration together with the POD method. The main advantage lies in the fact that the coarse propagator's spatial discretization becomes increasingly accurate as iterations proceed, while maintaining low computational cost.

Furthermore, as stated in the end of subsection 4.1, this method can also be interpreted as a parareal based adaptive POD method. When using the POD method to solve time-dependent partial differential equations, if the initial snapshots fail to capture the solution's behavior over the entire time interval, the numerical errors will increase rapidly over time. Our method can be viewed as an adaptive POD method which uses the data obtained by fine propagator in each time subinterval during the parareal iteration together with POD method to construct the subspace for spatial discretization.

We have applied our methods to two typical 3D advection-diffusion equations, the Kolmogorov flow and the ABC flow. Numerical results show both the effectiveness and accuracy of our method in simulating long-term evolution. Furthermore, we would like to emphasize that our method performs well for the advection-dominated cases. In our future work, we will focus on designing more efficient coarse propagators, improving updating strategies, and applying this method to other types of time-dependent partial differential equations.

Acknowledgments

The authors would like to thank Professor Aihui Zhou for his inspiring discussions during the early stages of this research and his valuable suggestions during the writing of this manuscript.

References

- [1] The toolbox Parallel Hierarchical Grid (PHG). <http://lsec.cc.ac.cn/phg/>, 2019.
- [2] Vincent Acary and Bernard Brogliato. Implicit Euler numerical scheme and chattering-free implementation of sliding mode systems. *Systems & Control Letters*, 59(5):284–293, 2010.
- [3] Leonardo Baffico, Stephane Bernard, Yvon Maday, Gabriel Turinici, and Gilles Zérah. Parallel-in-time molecular-dynamics simulations. *Physical Review E*, 66(5):057701, 2002.
- [4] Guillaume Bal. On the convergence and the stability of the parareal algorithm to solve partial differential equations. In *Domain decomposition methods in science and engineering*, pages 425–432. Springer, 2005.

- [5] Guillaume Bal and Qi Wu. *Symplectic parareal*. Springer, 2008.
- [6] Peter Benner, Serkan Gugercin, and Karen Willcox. A survey of projection-based model reduction methods for parametric dynamical systems. *SIAM review*, 57(4):483–531, 2015.
- [7] Adel Blouza, Laurent Boudin, and Sidi Mahmoud Kaber. Parallel in time algorithms with reduction methods for solving chemical kinetics. *Communications in Applied Mathematics and Computational Science*, 5(2):241–263, 2011.
- [8] Vadim Borue and Steven A Orszag. Numerical study of three-dimensional Kolmogorov flow at high Reynolds numbers. *Journal of Fluid Mechanics*, 306:293–323, 1996.
- [9] Susanne C Brenner. *The mathematical theory of finite element methods*. Springer, 2008.
- [10] NH Brummell, F Cattaneo, and SM Tobias. Linear and nonlinear dynamo properties of time-dependent ABC flows. *Fluid Dynamics Research*, 28(4):237, 2001.
- [11] Kevin Carlberg, Lukas Brencher, Bernard Haasdonk, and Andrea Barth. Data-driven time parallelism via forecasting. *SIAM Journal on Scientific Computing*, 41(3):B466–B496, 2019.
- [12] Feng Chen, Jan S Hesthaven, and Xueyu Zhu. On the use of reduced basis methods to accelerate and stabilize the parareal method. *Reduced Order Methods for Modeling and Computational Reduction*, pages 187–214, 2014.
- [13] Francisco Chinesta, Antonio Huerta, Gianluigi Rozza, and Karen Willcox. Model reduction methods. *Encyclopedia of Computational Mechanics Second Edition*, pages 1–36, 2017.
- [14] Xiaoying Dai, Miao Hu, Jack Xin, and Aihui Zhou. An augmented subspace based adaptive proper orthogonal decomposition method for time dependent partial differential equations. *Journal of Computational Physics*, 514:113231, 2024.
- [15] Xiaoying Dai, Xiong Kuang, Jack Xin, and Aihui Zhou. Two-grid based adaptive proper orthogonal decomposition method for time dependent partial differential equations. *Journal of Scientific Computing*, 84:1–27, 2020.
- [16] Xiaoying Dai, Claude Le Bris, Frédéric Legoll, and Yvon Maday. Symmetric parareal algorithms for Hamiltonian systems. *ESAIM: Mathematical Modelling and Numerical Analysis*, 47(3):717–742, 2013.
- [17] Xiaoying Dai and Yvon Maday. Stable parareal in time method for first- and second-order hyperbolic systems. *SIAM Journal on Scientific Computing*, 35(1):A52–A78, 2013.

- [18] Charbel Farhat and Marion Chandesris. Time-decomposed parallel time-integrators: theory and feasibility studies for fluid, structure, and fluid-structure applications. *International Journal for Numerical Methods in Engineering*, 58(9):1397–1434, 2003.
- [19] Paul F Fischer, Frédéric Hecht, and Yvon Maday. A parareal in time semi-implicit approximation of the Navier-Stokes equations. In *Domain decomposition methods in science and engineering*, pages 433–440. Springer, 2005.
- [20] Martin J Gander. 50 years of time parallel time integration. In *Multiple Shooting and Time Domain Decomposition Methods: MuS-TDD, Heidelberg, May 6-8, 2013*, pages 69–113. Springer, 2015.
- [21] Martin J Gander and Ernst Hairer. Nonlinear convergence analysis for the parareal algorithm. In *Domain decomposition methods in science and engineering XVII*, pages 45–56. Springer, 2008.
- [22] Martin J Gander, Yao-Lin Jiang, Bo Song, and Hui Zhang. Analysis of two parareal algorithms for time-periodic problems. *SIAM Journal on Scientific Computing*, 35(5):A2393–A2415, 2013.
- [23] Martin J Gander and Stefan Vandewalle. Analysis of the parareal time-parallel time-integration method. *SIAM Journal on Scientific Computing*, 29(2):556–578, 2007.
- [24] Martin J Gander, Shu-Lin Wu, and Tao Zhou. Time parallelization for hyperbolic and parabolic problems. *Acta Numerica*, 34:385–489, 2025.
- [25] Izaskun Garrido, Magne S Espedal, and Gunnar E Fladmark. A convergent algorithm for time parallelization applied to reservoir simulation. In *Domain decomposition methods in science and engineering*, pages 469–476. Springer, 2005.
- [26] Gene H Golub and Charles F Van Loan. *Matrix computations*. JHU press, 2013.
- [27] Abdul Qadir Ibrahim, Sebastian Götschel, and Daniel Ruprecht. Parareal with a physics-informed neural network as coarse propagator. In *European Conference on Parallel Processing*, pages 649–663. Springer, 2023.
- [28] Abdul Qadir Ibrahim, Sebastian Götschel, and Daniel Ruprecht. Space-time parallel scaling of parareal with a fourier neural operator as coarse propagator. *arXiv preprint arXiv:2404.02521*, 2024.
- [29] Frédéric Legoll, Tony Lelièvre, and Upanshu Sharma. An adaptive parareal algorithm: application to the simulation of molecular dynamics trajectories. *SIAM Journal on Scientific Computing*, 44(1):B146–B176, 2022.
- [30] Jacques-Louis Lions, Yvon Maday, and Gabriel Turinici. Résolution d’EDP par un schéma en temps pararéel. *Comptes Rendus de l’Académie des Sciences-Series I-Mathematics*, 332(7):661–668, 2001.

- [31] Y. Maday. Reduced basis method for the rapid and reliable solution of partial differential equations. *Proceedings of International Conference of Mathematicians, European Mathematical Society*, III:1255–1270, 2006.
- [32] Yvon. Maday. The parareal in time algorithm. In F. Magoulès, editor, *Substructuring Techniques and Domain Decomposition Methods*, chapter 2, pages 19–44. Saxe-Coburg Publications, Stirlingshire, UK, 2010.
- [33] Yvon Maday and Olga Mula. An adaptive parareal algorithm. *Journal of Computational and Applied Mathematics*, 377:112915, 2020.
- [34] Yvon Maday and Gabriel Turinici. Parallel in time algorithms for quantum control: Parareal time discretization scheme. *International Journal of Quantum Chemistry*, 93(3):223–228, 2003.
- [35] Allan S Nielsen. Feasibility study of the parareal algorithm. *Technical University of Denmark*, 2012.
- [36] AM Obukhov. Kolmogorov flow and its laboratory simulation. *Usp. Mat. Nauk*, 38(4):101–111, 1983.
- [37] SJP Pamela, N Carey, J Brandstetter, R Akers, L Zanisi, J Buchanan, V Gopakumar, M Hoelzl, G Huijsmans, K Pentland, T James, T Antonucci, and the JOREK Team. Neural-parareal: Dynamically training neural operators as coarse solvers for time-parallelisation of fusion MHD simulations. *arXiv preprint arXiv:2405.01355*, 2024.
- [38] René Pinnau. Model reduction via Proper Orthogonal Decomposition. In *Model Order Reduction: Theory, Research Aspects and Applications*, pages 95–109. Springer, 2008.
- [39] Gunnar Andreas Staff and Einar M Rønquist. Stability of the parareal algorithm. In *Domain decomposition methods in science and engineering*, pages 449–456. Springer, 2005.
- [40] John C Strikwerda. *Finite difference schemes and partial differential equations*. SIAM, 2004.
- [41] Rüdiger Verfürth. *A posteriori error estimation techniques for finite element methods*. OUP Oxford, 2013.
- [42] Stefan Volkwein. Model reduction using proper orthogonal decomposition. *Lecture Notes, Institute of Mathematics and Scientific Computing, University of Graz*, 1025, 2011.
- [43] Jack Xin, Yifeng Yu, and Andrej Zlatoš. Periodic orbits of the ABC flow with $A = B = C = 1$. *SIAM Journal on Mathematical Analysis*, 48(6):4087–4093, 2016.